Photonic Band Gaps Based on Tetragonal Lattices of Slanted Pores

Ovidiu Toader,[1] Mona Berciu,[2] and Sajeev John[1]

[1]*Department of Physics, University of Toronto, 60 St. George Street, Toronto, Ontario, Canada M5S 1A7*
[2]*Department of Physics and Astronomy, University of British Columbia, Vancouver, British Columbia, Canada V6T 1Z1*

(Received 16 December 2002; published 10 June 2003)

We describe broad new classes of three-dimensional (3D) structures which, when made of silicon, exhibit robust 3D photonic band gaps of up to 25% of the gap center frequency. The proposed photonic crystals are readily amenable to very high precision microfabrication using established techniques such as x-ray lithography and template inversion. Each architecture consists of a set of oriented cylindrical pores emanating from a two-dimensional (2D) square lattice mask with a two-point basis. Large bandwidth, microcircuits for light may be incorporated within the resulting photonic band gaps using an intercalated 2D photonic crystal layer.

DOI: 10.1103/PhysRevLett.90.233901 PACS numbers: 42.70.Qs

Since the introduction of the photonic band gap (PBG) concept [1,2], one of the holy grails of the subject has been the design and synthesis of high quality materials with a large PBG, that are amenable to efficient, large scale microfabrication and into which circuits of light can be readily incorporated. Such optical circuits would operate using the principle of light localization [3,4], rather than total internal reflection for waveguiding, and would enable frequency selective control of spontaneous emission from nearby atoms and molecules [2,5–7]. The identification of the diamond lattice [8] as a primary candidate for a large 3D PBG has led to the design [9,10] and microfabrication [11–13] of woodpile-type structures. An alternative square spiral structure with a potentially larger 3D PBG [14,15] and amenable to efficient synthesis [16,17] has been realized more recently [18]. Likewise, self-assembly methods have achieved very large scale face-centered cubic (fcc) lattices of spheres with a high degree of perfection, but with a relatively small PBG [19,20]. Despite this intense activity, broad, important, and distinct classes of microstructures (exhibiting very large and robust 3D PBGs) remain unidentified. In this Letter, we delineate four new sets of architectures that are amenable to microfabrication using high-resolution techniques such as x-ray lithography [21]. Manufacturable with nanometer scale precision, our designs enable low loss optical circuitry for visible and near-infrared light on a large scale, PBG based microchip.

Early studies suggested the possibility of achieving a moderate sized 3D PBG, using a lattice of criss-crossing pores, oriented along the three primitive lattice vectors of the fcc lattice and emanating from a triangular mask lattice on the sample surface [22]. In principle, this crystal exhibits a 17% PBG when made from optimized air cylinders in a silicon background of dielectric constant $\varepsilon = 11.9$. While this structure has been fabricated for microwave applications, the corresponding semiconductor material with submicron diameter pores has proven impractical to achieve using reactive ion etching methods [23,24]. It is both difficult to drill directly into the semiconductor to more than a few microns depth and nearly impossible to maintain sharply defined cylinder shapes near the crossing points of the pores. A closely related (distorted fcc) structure [25] has been synthesized on a very large scale using photoelectrochemical etching [26,27] in silicon and various III-V semiconductors. In silicon, this structure involves a triangular lattice of etch pits on the (1,1,1) crystallographic surface. Photoelectrochemical etching then leads to a set of three pores (symmetrically placed on a 29.5° cone with respect to the surface normal) emanating from each etch pit. This entails a tetragonal distortion of the fcc lattice and the resulting PBG is only 8% of the gap center frequency when optimized [28]. Moreover, the photoelectrochemical etching process requires doping of the semiconductor, resulting in sometimes undesirable, free charge carriers in the resulting PBG material. Recently, a new approach to 3D photonic crystal synthesis has been proposed based on ultraviolet holography [29] in a polymer template. However, an architecture exhibiting a complete 3D PBG, using this approach, remains to be identified.

Until now, the use of x-ray lithography to create slanted pore (SP) photonic crystals has been restricted to polymers (photoresists) structured in a fcc lattice and 10 μm or larger scale pores [30–32]. No PBG occurs in these polymers because of their relatively low refractive index. In order to achieve a PBG, a double inversion of the polymer template is required. In the "LIGA" technique [21,30,32], the pores in the polymer template are infiltrated with a metal and the polymer is subsequently removed, yielding an "inverse" structure. This metallic photonic crystal can, in principle, be used as a second template for chemical vapor deposition of silicon throughout its void regions. As in the case of inverse opals [19], selective etching of the metal template yields the desired "direct" structure (replica of the original polymer template), now consisting of air pores in a silicon background. The reduction in feature size, to create a

PBG centered at a wavelength of 1.5 μm, using LIGA, requires the careful development of high quality (and high aspect ratio) masks which can stop the x rays from etching the polymer template in regions other than the desired pores.

In this Letter, we introduce four new architectures of **S**lanted **P**ore ($\mathbf{SP_n}$) photonic crystals consisting of $\mathbf{n} = 2, 4$ pores per unit cell. These surpass the PBGs attainable from structures in the $\mathbf{SP}_3$ (three pores) class studied previously [22–25,30,32]. In addition to having gaps as large as 25% of the gap center frequency, our new $\mathbf{SP_n}$ architectures involve fewer pore crossings and therefore are less prone to disorder-induced degradation of the PBG. $\mathbf{SP_n}$ photonic crystals are defined using a 2D lattice (mask) and **n** pore axes associated with each unit cell of the mask lattice. In each of our $\mathbf{SP_n}$ architectures, the mask lattice has a two-point basis. After the required pores are drilled in prescribed orientation(s) through the lattice of mask holes, corresponding to one member of the basis, the mask is shifted to expose the second member of the basis, and the second set of oriented pores is drilled in the polymer photoresist. Figure 1 shows a $\mathbf{SP}_2$ structure constructed from a square lattice mask with primitive vectors $\vec{\mathbf{a}}_1$ and $\vec{\mathbf{a}}_2$, of length $\underline{\mathbf{a}}$. $\vec{\mathbf{c}}$ is an independent vector, of length $\underline{\mathbf{c}}$, perpendicular to the mask plane which, together with $\vec{\mathbf{a}}_1$ and $\vec{\mathbf{a}}_2$, define the tetragonal 3D unit cell. We define a pore, in a given unit cell containing the point **P** (see Fig. 1), by its orientation vector $n_1\vec{\mathbf{a}}_1 + n_2\vec{\mathbf{a}}_2 + \vec{\mathbf{c}}$ (n_1 and n_2 are integers) and its displacement vector $\vec{\delta} = \delta_1\vec{\mathbf{a}}_1 + \delta_2\vec{\mathbf{a}}_2$ ($0 \le \delta_1, \delta_2 < 1$) from the point **P** in the mask plane. We denote this pore by the symbol $[n_1, n_2]^{(\delta_1,\delta_2)}$ or simply $[n_1, n_2]$ when $\vec{\boldsymbol{\delta}} = 0$. The $\mathbf{SP}_2$ structure shown in Fig. 1 contains (in each 3D unit cell) a [1,1] pore emanating from **P** and a $[-1, 1]^{(0,0.5)}$ pore emanating from $\mathbf{P} + \vec{\boldsymbol{\delta}}$. This $\mathbf{SP}_2$ structure belongs to a family of 3D photonic crystals which we denote by the symbol $\mathbf{S}/[1, 1] \oplus [-1, 1]^{(0,0.5)}$, where **S** stands for **S**quare mask. The polymer template for this structure can be synthesized using two steps of x-ray lithography and a single mask. The ratio of tetragonal lattice parameters $\underline{\mathbf{c}}/\underline{\mathbf{a}}$ and the pore radius $\underline{\mathbf{r}}/\underline{\mathbf{a}}$ are variational parameters which span the family of $\mathbf{S}/[1, 1] \oplus [-1, 1]^{(0,0.5)}$ photonic crystals. The optimized photonic crystal in each family refers to the choice of variational parameters which yield the largest complete 3D PBG. For the $\mathbf{S}/[1, 1] \oplus [-1, 1]^{(0,0.5)}$ family with air pores in silicon ($\varepsilon = 11.9$), the optimized parameters are $\underline{\mathbf{c}} = \underline{\mathbf{a}}$ and $\underline{\mathbf{r}} = 0.3\underline{\mathbf{a}}$. The air volume filling fraction in this optimized crystal is 78.8% and the resulting PBG spans 20% of the gap center frequency.

A larger (24%) 3D PBG is attainable through a simple modification of the pore architecture described above. $\mathbf{S}/[1, 1] \oplus [-1, -1]^{(0.5,0)}$ is a distinct $\mathbf{SP}_2$ family which differs from $\mathbf{S}/[1, 1] \oplus [-1, 1]^{(0,0.5)}$ in the orientation and shift of the second set of pores. The inset of Fig. 2 shows the two masks, displaced by $(0.5\underline{\mathbf{a}}, 0)$, and the directions of the two sets of pores for the $\mathbf{S}/[1, 1] \oplus [-1, -1]^{(0.5,0)}$ family. The optimized structure in this case is characterized by $\underline{\mathbf{c}} = 1.40\underline{\mathbf{a}}$ and $\underline{\mathbf{r}} = 0.345\underline{\mathbf{a}}$. For this geometry, the

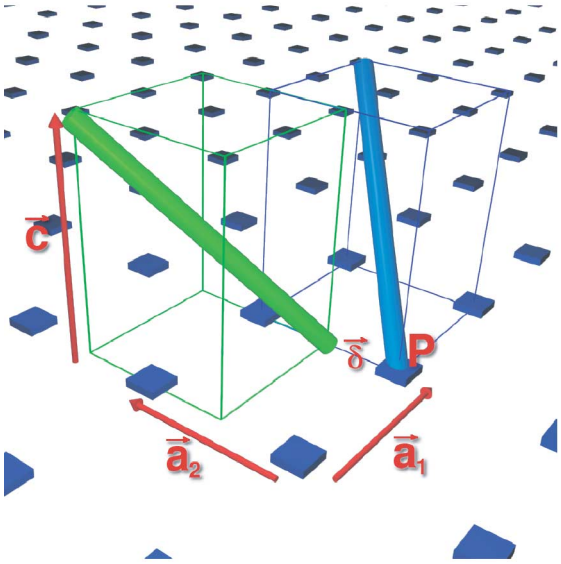

FIG. 1 (color online). An example of a $\mathbf{SP}_2$ structure based on a square mask of lattice constant $\underline{\mathbf{a}}$. $\vec{\mathbf{a}}_1$ and $\vec{\mathbf{a}}_2$ are the primitive vectors of the mask lattice and $\vec{\mathbf{c}}$ is a vector of length $\underline{\mathbf{c}}$ perpendicular to the mask plane. Associated with mask point **P** are two pore axes. The first runs from $\vec{\mathbf{0}}$ to $1\vec{\mathbf{a}}_1 + 1\vec{\mathbf{a}}_2 + \vec{\mathbf{c}}$ and the second from $\vec{\delta} = 0\vec{\mathbf{a}}_1 + 0.5\vec{\mathbf{a}}_2$ to $\vec{\delta} - 1\vec{\mathbf{a}}_1 + 1\vec{\mathbf{a}}_2 + \vec{\mathbf{c}}$. This $\mathbf{SP}_2$ structure belongs to the family $\mathbf{S}/[1, 1] \oplus [-1, 1]^{(0,0.5)}$.

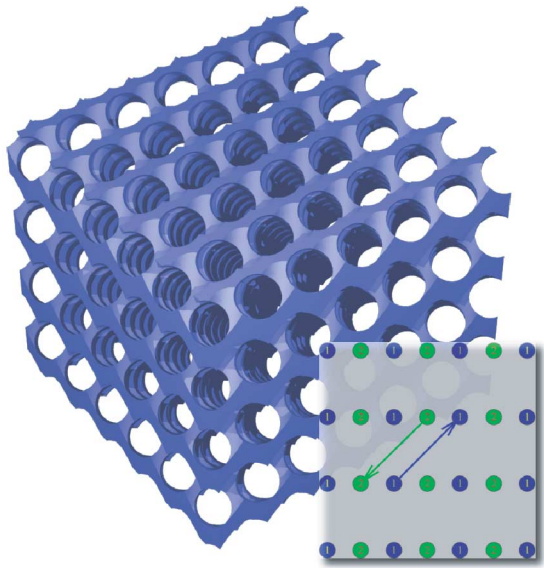

FIG. 2 (color online). The optimized silicon $\mathbf{S}/[1, 1] \oplus [-1, -1]^{(0.5,0)}$ photonic crystal. The radius of the pores is $\underline{\mathbf{r}} = 0.345\underline{\mathbf{a}}$ and $\underline{\mathbf{c}} = 1.40\underline{\mathbf{a}}$. The volume filling fraction of the pores is 80.16% and the full photonic band gap has a relative size of 24%. The inset shows the top view of the pores configuration for the $\mathbf{S}/[1, 1] \oplus [-1, -1]^{(0.5,0)}$ family.

volume filling fraction of the pores is 80.16% and the full photonic band gap, centered at $\omega\underline{\mathbf{a}}/2\pi c = \underline{\mathbf{a}}/\lambda_{\text{vac}} = 0.41$ (c is the speed of light), has a relative size of $\Delta\omega/\omega = 24\%$ in silicon ($\varepsilon = 11.9$). Figure 2 provides a three-dimensional perspective of the optimized $\mathbf{S}/[1,1] \oplus [-1,-1]^{(0.5,0)}$ photonic crystal. For the specific choice of $\underline{\mathbf{c}} = \sqrt{2}\underline{\mathbf{a}}$, the $\mathbf{S}/[1,1] \oplus [-1,-1]^{(0.5,0)}$ structure has some common features with an inverted "woodpile" crystal, comprised of circular air rods in a solid background. While the cylinder axes do not cross each other, there is overlap between the cylinders for the optimized radius, $\underline{\mathbf{r}} = 0.345\underline{\mathbf{a}}$, which leads to a larger PBG than conventional woodpile structures created through layer by layer growth [12,13]. Moreover, the PBG of the $\mathbf{S}/[1,1] \oplus [-1,-1]^{(0.5,0)}$ photonic crystal is very robust to deviations of the structural parameters from their optimum values. For $c = 1.40\underline{\mathbf{a}}$, a PBG of more than 20% exists for $0.30\underline{\mathbf{a}} < \underline{\mathbf{r}} < 0.38\underline{\mathbf{a}}$ and remains nonzero for the broad range $0.20\underline{\mathbf{a}} < \underline{\mathbf{r}} < 0.42\underline{\mathbf{a}}$. Likewise for $\underline{\mathbf{r}} = 0.345\underline{\mathbf{a}}$, a PBG of more than 20% exists throughout the range $1.1\underline{\mathbf{a}} < \underline{\mathbf{c}} < 1.7\underline{\mathbf{a}}$, corresponding to relative angle between pores ranging from 80° to 105°. For $\underline{\mathbf{r}} = 0.345\underline{\mathbf{a}}$, the PBG remains nonzero for a relative angle in the very broad range of 66° to 115°. In contrast, the PBG of the optimized conventional "woodpile," grown layer by layer with rods of rectangular cross section, is only 18% ($\varepsilon = 11.9$) and less robust.

Figure 3 shows the photonic band structure of the optimized $\mathbf{S}/[1,1] \oplus [-1,-1]^{(0.5,0)}$ crystal described above, calculated using an expansion with more than 2600 plane waves [8]. The full photonic band gap of 24% is centered at $\underline{\mathbf{a}}/\lambda_{\text{vac}} = 0.41$ and opens between bands 4 and 5 of the tetragonal photonic band structure. We have also studied the "inverted" $\mathbf{S}/[1,1] \oplus [-1,-1]^{(0.5,0)}$ family which consists of solid pores ($\varepsilon = 11.9$) in air. The optimized photonic crystal, in this case, is characterized by $\underline{\mathbf{c}} = 1.55\underline{\mathbf{a}}$ and $\underline{\mathbf{r}} = 0.19$. The volume filling fraction of the pores is 30.6% and the relative size of the full photonic band gap is 17%. This gap also opens between bands 4 and 5 and is centered at $\underline{\mathbf{a}}/\lambda_{\text{vac}} = 0.35$.

The two distinct PBG architectures described above, belonging to the $\mathbf{SP}_2$ class with square mask, are both geometrically simpler than the $\mathbf{SP}_3$ structures with a triangular mask [21–24] and yield larger and more robust gaps than the widely studied woodpile structure [9–13]. Even larger PBGs than the $\mathbf{SP}_2$ class are achieved by photonic crystals in the $\mathbf{SP}_4$ class. An example of such an $\mathbf{SP}_4$ crystal is the one denoted by $\mathbf{S}_{4p}^{(1)} \equiv \mathbf{S}/([1,1] \oplus [1,-1]) \oplus ([-1,-1] \oplus [-1,1])^{(0.5,0)}$ and illustrated in Fig. 4. Depicted in the inset of Fig. 4 are the same square lattice masks used previously for the $\mathbf{SP}_2$ structures except with two pores per mask point and, consequently, four pores per 3D unit cell. The optimized $\mathbf{S}_{4p}^{(1)}$ crystal is characterized by $\underline{\mathbf{c}} = 1.1\underline{\mathbf{a}}$ and $\underline{\mathbf{r}} = 0.31\underline{\mathbf{a}}$, corresponding to a pore (air) volume filling fraction of 81.51%. For a background material with $\varepsilon = 11.9$, the photonic band gap spans 25% and is centered at $\underline{\mathbf{a}}/\lambda_{\text{vac}} = 0.47$. For $\underline{\mathbf{r}} = 0.31\underline{\mathbf{a}}$, a gap of more than 20% is found for $\underline{\mathbf{a}} < \underline{\mathbf{c}} < 1.55\underline{\mathbf{a}}$ and remains nonzero for the very broad range of $0.8\underline{\mathbf{a}} < \underline{\mathbf{c}} < 2.15\underline{\mathbf{a}}$. For $\underline{\mathbf{c}} = 1.1\underline{\mathbf{a}}$ a gap of more than 20% exists for $0.26\underline{\mathbf{a}} < \underline{\mathbf{r}} < 0.34\underline{\mathbf{a}}$ and remains nonzero for the very broad range of $0.18\underline{\mathbf{a}} < \underline{\mathbf{r}} < 0.38\underline{\mathbf{a}}$. We have also identified a second family of $\mathbf{SP}_4$ crystals exhibiting a large 3D PBG. This distinct family is denoted by $\mathbf{S}_{4p}^{(2)} \equiv \mathbf{S}/([1,1] \oplus [1,-1]) \oplus ([-1,-1] \oplus [-1,1])^{(0.5,0.5)}$ and is characterized by the same set of four pore orientations as $\mathbf{S}_{4p}^{(1)}$, but a distinct basis vector (mask translation)

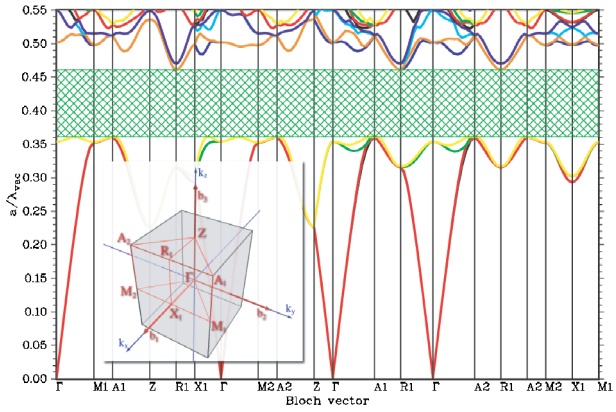

FIG. 3 (color online). Band structure for the optimized $\mathbf{S}/[1,1] \oplus [-1,-1]^{(0.5,0)}$ photonic crystal ($\varepsilon = 11.9$). The crystal is characterized by $\underline{\mathbf{c}} = 1.40\underline{\mathbf{a}}$ and $\underline{\mathbf{r}} = 0.345\underline{\mathbf{a}}$. The full photonic band gap is centered at $\underline{\mathbf{a}}/\lambda_{\text{vac}} = 0.41$, opens between bands 4 and 5 of the tetragonal photonic band structure, and its relative size is 24%. The positions of the irreducible Brillouin zone symmetry points are illustrated in the inset.

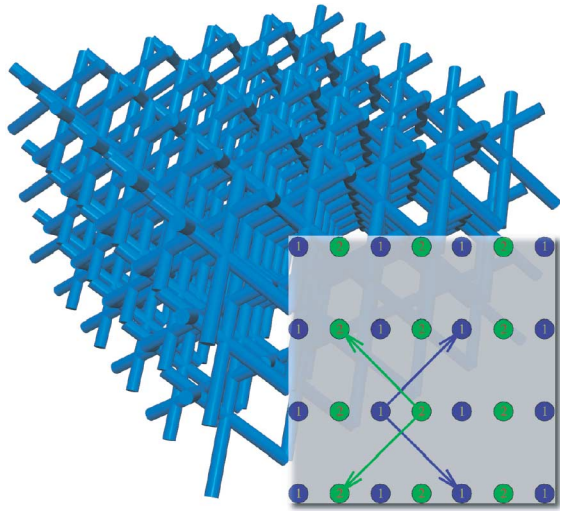

FIG. 4 (color online). The network formed by the pores of the $\mathbf{S}_{4p}^{(1)}$ structure. The photonic crystal illustrated corresponds to $\underline{\mathbf{r}} = 0.08\underline{\mathbf{a}}$ and $\underline{\mathbf{c}} = 1.1\underline{\mathbf{a}}$. The inset displays the two masks and the pores configuration for the entire $\mathbf{S}_{4p}^{(1)}$ family.

$\vec{\delta} = 0.5\vec{\mathbf{a}}_1 + 0.5\vec{\mathbf{a}}_2$. The optimized $\mathbf{S}_{4p}^{(2)}$ crystal, characterized by $\underline{\mathbf{c}} = \underline{\mathbf{a}}$ and $\underline{\mathbf{r}} = 0.29\underline{\mathbf{a}}$, has a photonic band gap of 22% which is also robust to changes in $\underline{\mathbf{c}}$ and $\underline{\mathbf{r}}$.

The LIGA method can be adapted to create point defects and optical waveguide channels within each of the four $\mathbf{SP_n}$ photonic crystal families described above. An optical microchip (containing prepatterned optical circuitry), in the form of a planar defect layer, may be introduced at the initial template stage by means of a "negative" photoresist that is impervious to the x rays used to etch the "positive" photoresists in the discussion above. The template for the microchip consists of a thin (roughly $0.5\underline{\mathbf{a}}$) membrane of negative photoresist which has been independently prepatterned as a 2D photonic crystal with the periodicity of the mask lattices shown in Figs. 1, 2, and 4. Desired waveguide channels and microcavity defects may also be prepatterned on this 2D, negative resist, membrane. The prepatterned negative photoresist is then sandwiched between a pair of unpatterned positive photoresists of thickness, roughly $5\underline{\mathbf{c}}$. After suitable alignment of an x-ray mask, the sandwich structure is now patterned as a $\mathbf{SP}_2$ or $\mathbf{SP}_4$ lattice in the regions of positive photoresist (as described above) by x-ray lithography. The template can then be replicated with silicon using the double inversion procedure described above. It has been demonstrated [33] that the optical waveguide modes of the membrane, if designed appropriately, will fall within the 3D PBG of the cladding layers, enabling broadband, lossless and diffractionless, flow of light within the microchip.

In summary, we have carried out an exhaustive study of slanted pore photonic crystals and identified four broad, new architectures for very large 3D photonic band gaps in the near-infrared (1.5 μm), suitable for ultrahigh-resolution lithography. These architectures achieve close to the largest photonic band gaps ever predicted [34] without the undesirable complexities of diamond lattice microfabrication. Given the prospect for nanometer scale precision in microfabrication, these PBG materials may open the door to nearly lossless optical microcircuitry and a variety of novel quantum optical effects [6,7] involving photons and atoms placed within these structures.

This work was supported in part by the Natural Sciences and Engineering Research Council of Canada. M. B. acknowledges the hospitality of the University of Toronto, where this work was carried out.

[1] S. John, Phys. Rev. Lett. **58**, 2486 (1987).
[2] E. Yablonovitch, Phys. Rev. Lett. **58**, 2059 (1987).
[3] S. John, Phys. Rev. Lett. **53**, 2169 (1984).
[4] S. John, Phys. Today **44**, No. 5, 32 (1991).
[5] V. P. Bykov, Sov. J. Quantum Electron. **4**, 861 (1975).
[6] S. John and J. Wang, Phys. Rev. Lett. **64**, 2418 (1990).
[7] S. John and M. Florescu, J. Opt. A **3**, S103 (2001).
[8] K. M. Ho, C. T. Chan, and C. M. Soukoulis, Phys. Rev. Lett. **65**, 3152 (1990).
[9] C. T. Chan *et al.*, Solid State Commun. **89**, 413 (1994).
[10] H. S. Sözüer and J. P. Dowling, J. Mod. Opt. **41**, 231 (1994).
[11] E. Özbay *et al.*, Appl. Phys. Lett. **64**, 2059 (1994).
[12] S. Y. Lin *et al.*, Nature (London) **394**, 251 (1998).
[13] S. Noda *et al.*, Science **289**, 604 (2000).
[14] O. Toader and S. John, Science **292**, 1133 (2001).
[15] O. Toader and S. John, Phys. Rev. E **66**, 016610 (2002).
[16] K. Robbie, Maichael J. Brett, and A. Lakhtakia, J. Vac. Sci. Technol. **13**, 2991 (1995).
[17] K. Robbie, M. J. Brett, and A. Lakhtakia, Nature (London) **384**, 616 (1996).
[18] Scott R. Kennedy *et al.*, Nano Lett. **2**, 59 (2002).
[19] A. Blanco *et al.*, Nature (London) **405**, 437 (2000).
[20] H. Miguez *et al.*, Adv. Mater. **13**, 1634 (2001).
[21] W. Ehrfeld and A. Schmidt, J. Vac. Sci. Technol. B **16**, 3526 (1998).
[22] E. Yablonovitch, T. J. Gmitter, and K. M. Leung, Phys. Rev. Lett. **67**, 2295 (1991).
[23] C. C. Cheng and A. Scherer, J. Vac. Sci. Technol. B **13**, 2696 (1995).
[24] C. C. Cheng *et al.*, J. Vac. Sci. Technol. B **14**, 4110 (1996).
[25] M. Christophersen *et al.*, Mater. Sci. Eng. B **69**, 194 (2000).
[26] S. Ottow, V. Lehmann, and H. Föll, Appl. Phys. A **63**, 153 (1996).
[27] A. Birner *et al.*, Adv. Mater. **13**, 377 (2001).
[28] T. Chan and S. John (to be published).
[29] M. Campbell *et al.*, Nature (London) **404**, 53 (2000).
[30] C. Cuisin *et al.*, Opt. Quantum Electron. **34**, 13 (2002).
[31] K.-H. Brenner *et al.*, Appl. Opt. **32**, 6464 (1993).
[32] G. Feiertag *et al.*, Appl. Phys. Lett. **71**, 1441 (1997).
[33] A. Chutinan, S. John, and O. Toader, Phys. Rev. Lett. **90**, 123901 (2003).
[34] C. T. Chan, S. Datta, K. M. Ho, and C. M. Soukoulis, Phys. Rev. B **50**, 1988 (1994)